OTFS Modulation in Dual-LED Indoor Visible Light Communication Systems

Sujata Sinha and A. Chockalingam
Department of ECE, Indian Institute of Science, Bangalore 560012

Abstract—In this paper, we investigate the use of a new modulation scheme recently introduced in the RF domain, called orthogonal time frequency space (OTFS) modulation, in an indoor visible light communication (VLC) setting. In particular, we consider VLC systems that employ dual-LED schemes for transmission. The following dual-LED schemes are considered: 1) non-DC biased (NDC) scheme, and 2) dual-LED complex modulation (DCM) scheme. The proposed NDC-OTFS scheme uses 2-dimension (2D) Hermitian symmetry operation to convert complex signals to positive, real-valued signals suitable for transmission in the optical domain, and the proposed DCM-OTFS scheme achieves this by exploiting the polar representation of complex signals. We obtain analytical upper bounds on the bit error performance of the proposed NDC-OTFS and DCM-OTFS schemes, which are found to be tight at high signal-to-noise ratios (SNR). Our analytical and simulation results show that the proposed NDC-OTFS and DCM-OTFS schemes achieve better performance, respectively, compared to NDC-OFDM and DCM-OFDM schemes known in the VLC literature. Further, using the ratio of the minimum distance of different normalized received signal sets as a metric, we quantify the spatial distribution of the SNR gain of the proposed NDC-OTFS/DCM-OTFS schemes compared to NDC-OFDM/DCM-OFDM schemes.

Keywords: OTFS modulation, visible light communication, dual-LED schemes, NDC-OTFS, DCM-OTFS.

I. INTRODUCTION

Visible light communication (VLC) technology is emerging as an attractive complementary technology to radio frequency (RF) technology for wireless communications in indoor and vehicular environments [1],[2]. VLC systems use light-emitting diodes (LED) as wireless transmitters and photodiodes (PDs) as wireless receivers. Several researchers have investigated modulation and signal processing techniques for VLC [3], including multiple-input multiple-output (MIMO) techniques using real signal sets such as M-ary pulse amplitude modulation (PAM) with positive-valued signal points [3],[4],[5]. Also, the use of orthogonal frequency division multiplexing (OFDM) techniques suited for VLC has been an area of interest for researchers [6]-[12]. Techniques using complex modulation schemes such as M-ary quadrature amplitude modulation (QAM) along with OFDM using Hermitian symmetry has been studied extensively in DC-biased optical (DCO) OFDM [6], asymmetrically clipped optical (ACO) OFDM [7], flip OFDM [8], and non-DC-biased (NDC)

OFDM [9], [10]. These techniques use Hermitian symmetry to generate positive and real-valued signals for transmission. Multi-LED techniques without using Hermitian symmetry by exploiting the spatial domain for OFDM have been studied in quad-LED complex modulation (QCM) OFDM and dual-LED complex modulation (DCM) OFDM schemes [11], [12].

Recently, a new modulation scheme named orthogonal time frequency space (OTFS) modulation has been introduced in the RF communications domain in [13], where it has been shown that OTFS achieves significantly better performance compared to OFDM. OTFS is a two-dimensional (2D) signaling technique. MN information symbols are multiplexed in the delay-Doppler (DD) domain using M Doppler bins and N delay bins. These symbols in the DD domain are mapped to time domain using 2D transformations [14]. While OTFS is widely recognized for its superior performance in high-Doppler channels [13]-[16], it has been shown to perform very well in static multipath channels as well [17]. This motivates the investigation of OTFS for indoor VLC systems where the channel gains are often static.

Recently, in [18], OTFS has been studied for optical wireless communication (OWC) by considering a single-LED DC-biased optical (DCO) scheme along with OTFS. This study has revealed that DCO-OTFS can perform better than conventional DCO-OFDM in OWC systems. We note that investigation of OTFS modulation in VLC systems is both nascent and promising, and the topic needs significant research attention. Recognizing this, in this paper, we investigate OTFS modulation in the context of multi-LED VLC systems. OTFS modulation in multi-LED VLC systems has not been reported in the literature thus far. Multi-LED and multi-PD VLC systems (similar to MIMO systems in RF domain) are important as they offer increased rate and performance benefits. In this paper, we consider two promising dual-LED architectures that eliminate the need for Hermitian symmetry and DC-bias. The first architecture is non-DC-biased (NDC) scheme which uses two LEDs for transmission, where a 2D Hermitian operation converts complex modulation symbols into real valued signals, and one LED is meant for sending positive-valued signals and another LED is meant for sending the magnitude of negative-valued signals. In the process, this scheme avoids the need for DC-bias and its optimization to obtain positive-valued signals for optical transmission. The second architecture is dual-LED complex modulation (DCM) scheme which uses one LED to send the magnitude and another LED to send the phase of complex modulation signals. This architecture eliminates

the need for both Hermitian operation and DC-bias. Our new contributions in this paper can be summarized as follows.

- We propose NDC-OTFS and DCM-OTFS schemes for VLC systems and obtain analytical upper bounds on the bit error performance of the proposed schemes. The bounds are found to be tight at high signal-to-noise ratios (SNR).
- Our analytical and simulation results show that the proposed NDC-OTFS and DCM-OTFS schemes achieve better performance, respectively, compared to NDC-OFDM and DCM-OFDM schemes known in the VLC literature.
- Using the ratio of the minimum distance of different normalized received signal sets as a metric, we quantify the spatial distribution of the SNR gain/loss of the proposed NDC-OTFS/DCM-OTFS schemes compared to the NDC-OFDM/DCM-OFDM schemes.

Notations: We have used x, $\mathbf{x}$, and $\mathbf{X}$ to denote scalar, vector and matrix, respectively. Also, $\mathbf{F}_M = \left\{ \frac{1}{\sqrt{M}} e^{2\pi j \frac{ml}{M}} \right\}_{m,l=0}^{M-1}$ and $\mathbf{F}_M^H$ denote the M-point DFT and IDFT matrices, respectively.

The rest of the paper is organized as follows. The indoor VLC system model is presented in Sec II. The proposed NDC-OTFS and DCM-OTFS schemes are presented in Sec. III. Performance analysis and simulation results are presented in Secs. IV and V. Conclusions are presented in Sec. VI.

II. INDOOR VLC SYSTEM MODEL

We consider an indoor VLC system with N_t transmitting LEDs and N_r receiving PDs in a room of dimension 5m × 5m × 3.5m as shown in Fig. 1. The LEDs are placed 0.5m below the ceiling and the PDs are placed 0.8m above the ground on a table. Each LED is either OFF or emits some intensity whose magnitude is based on the complex modulated symbol sent in each channel use. The proposed NDC-OTFS and DCM-OTFS schemes are block transmission schemes that employ multiple channel uses (say, T channel uses) for transmission. Let $\mathbf{X}$ denote the $N_t \times T$ transmit matrix, given by

$$\mathbf{X} = \begin{bmatrix} x[1,1] & x[1,2] & \cdots & x[1,T] \\ x[2,1] & x[2,2] & \cdots & x[2,T] \\ \vdots & \vdots & \ddots & \vdots \\ x[N_t,1] & x[N_t,2] & \cdots & x[N_t,T] \end{bmatrix}, \quad (1)$$

where $x[j,t]$ denotes the intensity of light transmitted by the jth LED in the tth channel use. We assume the LEDs to have Lambertian radiation pattern [19]. We consider a static channel with line-of-sight (LOS) paths between the LEDs and the PDs. The channel matrix $\mathbf{H}$ is of the order $N_r \times N_t$, whose (i,j)th element h_{ij} is the LOS channel gain between the jth LED and ith PD, which is given by [1]

$$h_{ij} = \frac{n+1}{2\pi} \cos^n \phi_{ij} \cos \theta_{ij} \frac{A}{d_{ij}^2} \operatorname{rect}\left(\frac{\theta_{ij}}{FOV} \right), \quad (2)$$

where n is the mode number of the LED radiation pattern, ϕ_{ij} is the angle of emergence from the jth LED towards the ith PD, A is the area of the PD, d_{ij} is the distance between
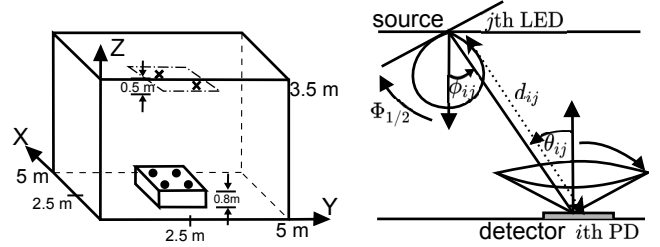

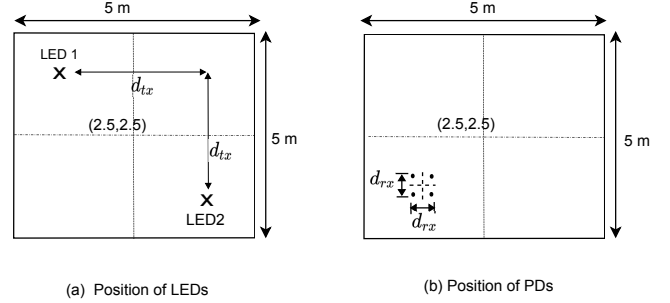Fig. 1: Indoor VLC system setup. A cross represents an LED and a dot represents a PD.

(a) Position of LEDs   (b) Position of PDs

Fig. 2: Location of the transmitter LEDs and the receiver PDs.

the jth LED and the ith PD, θ_{ij} is the angle of incidence at the ith LED from the jth LED, FOV is the field-of-view of the PD, and $\operatorname{rect}(x) = 0$, for all $|x| > 1$, where $|\cdot|$ represents the absolute value operator or cardinality of a set. The mode number is given by $n = \frac{-\ln(2)}{\ln \cos \Phi_{\frac{1}{2}}}$, where $\Phi_{\frac{1}{2}}$ is the half power semi-angle of the LED.

Assuming perfect channel knowledge and synchronisation at the receiver, the $N_r \times T$ received signal matrix $\mathbf{Y}$ can be written as

$$\mathbf{Y} = r\mathbf{H}\mathbf{X} + \mathbf{N}, \quad (3)$$

where r is the responsivity of the PD in Amps/Watt and $\mathbf{N}$ is the $N_r \times T$ noise matrix. Each element in $\mathbf{N}$ is real valued additive white Gaussian noise (AWGN) with zero mean and variance $\sigma^2 = \sigma_{shot}^2 + \sigma_{thermal}^2$, where σ_{shot}^2 is the shot noise variance and $\sigma_{thermal}^2$ is the thermal noise variance [20],[4]. The average SNR is given by $\bar{\gamma} = \frac{r^2}{\sigma^2 N_r} \sum_{i=1}^{N_r} \mathbb{E}[|\mathbf{h}_i\mathbf{X}|^2]$, where $\mathbf{h}_i$ is the ith row of $\mathbf{H}$.

The proposed NDC-OTFS and DCM-OTFS schemes (presented in the next section) use two transmit LEDs (i.e., $N_t = 2$). These LEDs are placed 0.5 m below the ceiling of the room as shown in Fig. 2(a), where the distance between the LEDs is given by $\sqrt{2}d_{tx}$. The placement of the receiver is as shown in Fig 2(b). The coordinate of the receiver location on the receiver plane (surface of the table which is 0.8 m above the ground) is denoted by (X_R, Y_R). The receiver is assumed to have $N_r = 4$ PDs placed at the corners of a square of side d_{rx} and center (X_R, Y_R). We will vary the location of the receiver in the receiver plane and obtain the spatial distribution of the system performance.

III. PROPOSED NDC-OTFS AND DCM-OTFS SCHEMES

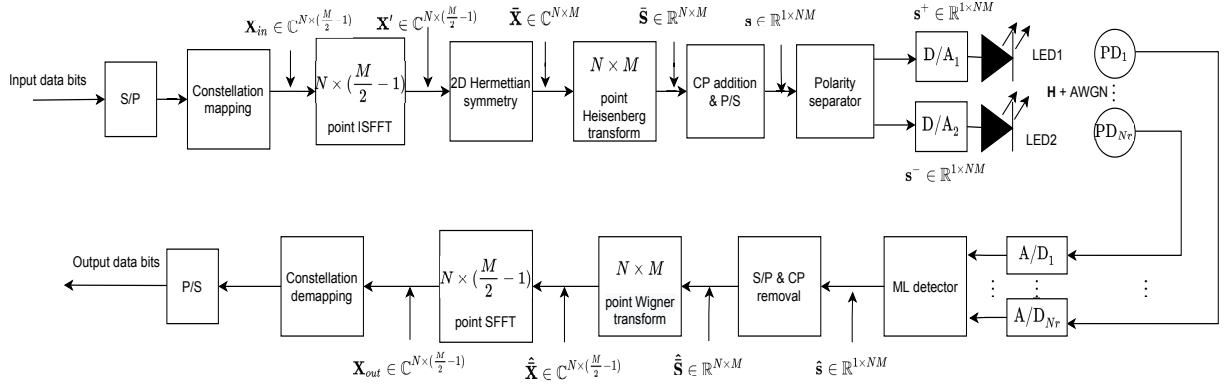In this section, we present the proposed NDC-OTFS and DCM-OTFS schemes.

Fig. 3: Proposed NDC-OTFS scheme.

A. Proposed NDC-OTFS scheme

The block diagram of the proposed NDC-OTFS scheme is shown in Fig. 3. $N(\frac{M}{2} - 1) \log_2 |\mathbb{A}|$ information bits are mapped to $N(\frac{M}{2} - 1)$ modulation symbols from a modulation alphabet $\mathbb{A}$ (e.g., QAM/PSK), where $|\mathbb{A}|$ is the alphabet size. These information symbols, denoted by $x[k,l]$, $k = 0, 1, \cdots, N-1$, $l = 1, \cdots, \frac{M}{2} - 1$, are populated in a matrix $\mathbf{X}_{in}$ of size $N \times (\frac{M}{2} - 1)$ in the DD domain. The matrix $\mathbf{X}_{in}$ is converted into a matrix $\mathbf{X}'$ in the time-frequency (TF) domain using $N \times (M/2 - 1)$-point (2D) inverse symplectic finite Fourier transform (ISFFT) operation. The (n, m)th element in $\mathbf{X}'$, denoted by $X'[n.m]$, is given by

$$X'[n,m] = \frac{2}{(M-2)N} \sum_{k=0}^{N-1} \sum_{l=0}^{M/2-2} x[k,l] e^{j2\pi \left(\frac{nk}{N} - \frac{2ml}{M-2} \right)}, \quad (4)$$

where $n = 0, 1, \cdots, N-1$ and $m = 1, \cdots, (\frac{M}{2} - 1)$. A 2D Hermitian symmetry operation is then carried out on $\mathbf{X}'$ to obtain the output matrix $\bar{\mathbf{X}}$ of size $N \times M$ as

$$\bar{\mathbf{X}} = \begin{bmatrix} 0 & X'[1,1] & \cdots & X'[1, \frac{M}{2} - 1] & 0 & X'^*[1, \frac{M}{2} - 1] & \cdots & X'^*[1,1] \\ 0 & X'[2,1] & \cdots & X'[2, \frac{M}{2} - 1] & 0 & X'^*[2, \frac{M}{2} - 1] & \cdots & X'^*[2,1] \\ \vdots & \vdots & \ddots & \vdots & \vdots & \vdots & \ddots & \vdots \\ 0 & X'[N,1] & \cdots & X'[N, \frac{M}{2} - 1] & 0 & X'^*[N, \frac{M}{2} - 1] & \cdots & X'^*[N,1] \end{bmatrix}.$$

The above Hermitian symmetry operation is carried out in order to ensure the output of the subsequent Heisenberg transform to be real and bipolar. The TF domain complex matrix $\bar{\mathbf{X}}$ is converted into a real matrix $\bar{\mathbf{S}}$ of size $N \times M$ in the time domain through $N \times M$ point Heisenberg transform using M-point IDFT [16], as

$$\bar{\mathbf{S}} = \sqrt{M} \mathbf{F}_M^H \bar{\mathbf{X}}^T, \quad (5)$$

The (n, m)th element of $\bar{\mathbf{S}}$, denoted by $\bar{S}[n,m]$, is given by

$$\bar{S}[n,m] = \frac{1}{\sqrt{M}} \sum_{m=0}^{M-1} \bar{X}[n,m] e^{j2\pi \frac{ml}{M}}. \quad (6)$$

The matrix $\bar{\mathbf{S}}$ is then converted into an NM-sized vector $\mathbf{s}$ through parallel-to-serial (P/S) conversion, and a cyclic prefix (CP) is added. The positive and negative elements in $\mathbf{s}$ are separated using a polarity separator. The output of the polarity separator are two NM-sized row vectors $\mathbf{s}^+$ and $\mathbf{s}^-$. Denoting the kth elements of $\mathbf{s}$, $\mathbf{s}^+$, and $\mathbf{s}^-$ as $s(k)$, $s^+(k)$, and $s^-(k)$, respectively, $s^+(k)$s and $s^-(k)$s are obtained as follows: 1) $s^+(k) = s(k)$ if $s(k) > 0$ and $s^+(k) = 0$ if $s(k) \leq 0$, and 2) $s^-(k) = -s(k)$ if $s(k) \leq 0$ and $s^-(k) = 0$ if $s(k) > 0$. The $\mathbf{s}^+$ and $\mathbf{s}^-$ vectors drive the LED1 and LED2, respectively. Note that due to the polarity separation operation above, at any given channel use, only one of the LEDs is on and the other LED is off, and there is no need for DC bias. Also, the simultaneous transmission of $\mathbf{s}^+$ and $\mathbf{s}^-$ vectors from LED1 and LED2 can be viewed as the transmission of a $2 \times MN$ matrix given by

$$\mathbf{S} = \begin{bmatrix} \mathbf{s}^+ \\ \mathbf{s}^- \end{bmatrix}. \quad (7)$$

It can be seen that $N(\frac{M}{2} - 1)$ symbols from the alphabet $\mathbb{A}$ are sent in MN channel uses in this scheme. Therefore, the achieved rate in bits per channel use (bpcu) is given by

$$\eta_{\text{ndc-otfs}} = \frac{M-2}{2M} \log_2 |\mathbb{A}| \text{ bpcu.} \quad (8)$$

Let $\mathbf{Y}$ denote the $N_r \times MN$ received signal matrix at the receiver corresponding to the transmit signal matrix $\mathbf{S}$. Then, $\mathbf{Y}$ can be written as

$$\mathbf{Y} = r\mathbf{H}\mathbf{S} + \mathbf{W}, \quad (9)$$

where $\mathbf{H}$ is the $N_r \times 2$ MIMO VLC channel matrix, $\mathbf{W}$ is the $N_r \times MN$ noise matrix, and r is the responsivity. Let $\mathbb{S}$ denote the set of all possible NDC-OTFS transmit signal matrices. The maximum likelihood (ML) decision rule can then be written as

$$\hat{\mathbf{S}}_{\text{ML}} = \underset{\mathbf{S} \in \mathbb{S}}{\arg\min} \|\mathbf{Y} - r\mathbf{H}\mathbf{S}\|^2. \quad (10)$$

The $\mathbf{s}$ vector corresponding to the detected matrix $\hat{\mathbf{S}}_{\text{ML}}$ is converted into matrix $\hat{\bar{\mathbf{S}}}$ of size $N \times M$ after removing the CP and serial-to-parallel (S/P) conversion. The matrix $\hat{\bar{\mathbf{S}}}$ is then converted into TF domain matrix $\hat{\bar{\mathbf{X}}}$ of size $N \times M$ using Wigner transform as

$$\hat{\bar{\mathbf{X}}} = \frac{1}{\sqrt{M}} \mathbf{F}_M \hat{\bar{\mathbf{S}}}, \quad (11)$$
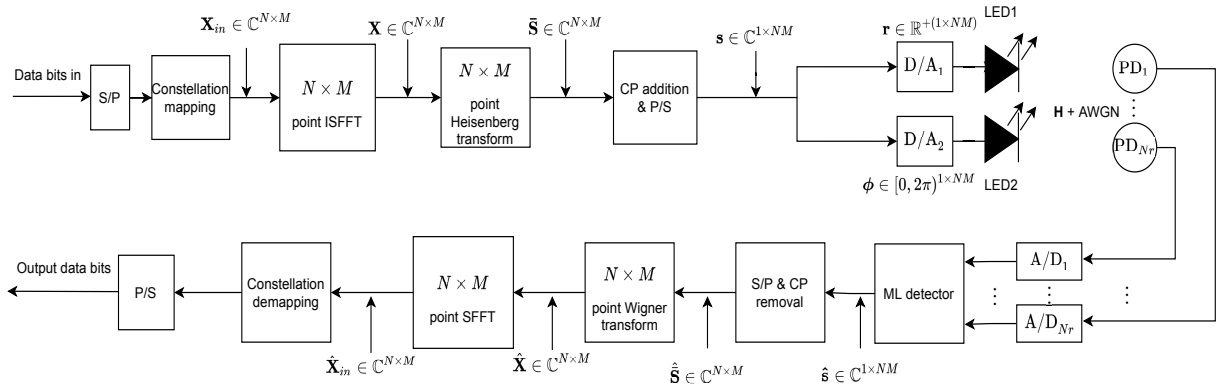
Fig. 4: Proposed DCM-OTFS scheme.

From $\hat{\bar{\mathbf{X}}}$, we take columns 1 to $M/2$ and perform $N(\frac{M}{2} - 1)$-point SFFT operation to form a matrix $\mathbf{X}_{out}$. The (k, l)th element of $\mathbf{X}_{out}$ is denoted by $\hat{x}[k, l]$, $k = 0, \cdots, N - 1$, $l = 1, \cdots, \frac{M}{2} - 2$, and is given by

$$\hat{x}[k, l] = \sum_{n=0}^{N-1} \sum_{m=0}^{M/2-1} \hat{\bar{X}}[n, m] e^{-j 2\pi \left(\frac{nk}{N} - \frac{2ml}{M-2} \right)}. \quad (12)$$

The $\hat{x}[k, l]$s are mapped to the nearest symbols in $\mathbb{A}$ which are demapped to the corresponding information bits.

B. Proposed DCM-OTFS scheme

The NDC-OTFS scheme proposed in the previous subsection has the advantage of no DC bias. It achieved this advantage through the use of dual LEDs and 2D Hermitian symmetry operation. The Hermitian symmetry operation, however, resulted in rate loss. In this subsection, we propose DCM-OTFS scheme which does not need Hermitian symmetery operation, and hence there is no rate loss. This scheme exploits the polar representation of complex signals. It uses two LEDs, one LED to transmit the amplitude and the other LED to transmit the phase of the OTFS modulated complex signals. Therefore, there is no need for DC bias as well.

The block diagram of the proposed DCM-OTFS scheme is shown in Fig. 4. Here, $NM \log_2 |\mathbb{A}|$ bits are first mapped into NM symbols from modulation alphabet $\mathbb{A}$. These information symbols are populated in a $N \times M$-sized matrix $\mathbf{X}_{in}$ in the DD domain, which is passed through $N \times M$ point ISFFT operation to obtain the signal matrix $\bar{\mathbf{X}}$ in the TF domain. This TF domain signal matrix is converted into the matrix $\bar{\mathbf{S}}$ in the time domain using Heisenberg transform.

The matrix $\bar{\mathbf{S}}$ is then converted into vector $\mathbf{s}$ by P/S conversion and adding CP. The vector $\mathbf{s}$ consists of complex elements, whose magnitudes and phases are transmitted through LED1 and LED2, respectively, as follows. Let the kth element of vector $\mathbf{s}$ be denoted by s_k. Then, s_k can be represented in polar form as $r_k e^{j\phi_k}$, where

$$\begin{aligned} r_k &= |s_k|, \quad r_k \in \mathbb{R}^+ \\ \phi_k &= \arg(s_k), \quad \phi_k \in [0, 2\pi). \end{aligned} \quad (13)$$

The r_ks and ϕ_ks are transmitted through LED1 and LED2, respectively. The simultaneous transmission of vectors $\mathbf{r} =$ $[r_1 \ r_2 \ ... \ r_{MN}]$ and $\boldsymbol{\phi} = [\phi_1 \ \phi_2 \ ... \ \phi_{MN}]$ from LED1 and LED2, respectively, can be viewed together as the transmission of a $2 \times NM$ matrix $\mathbf{S}$, given by

$$\mathbf{S} = \begin{bmatrix} \mathbf{r} \\ \boldsymbol{\phi} \end{bmatrix}. \quad (14)$$

As can be seen, in this scheme, NM information symbols are sent in NM channel uses. Therefore, the achieved rate in this scheme is given by

$$\eta_{\text{dcm-otfs}} = \log_2 |\mathbb{A}| \quad \text{bpcu}. \quad (15)$$

At the receiver, inverse operations as shown in Fig. 4 are carried out to recover the information bits.

IV. PERFORMANCE ANALYSIS

In this section, we obtain the upper bound on the bit error rate (BER) performance of the proposed schemes and a normalized minimum distance metric to compare the performance of different schemes.

A. Upper bound on BER

Consider the system model in (9) and the corresponding ML decision rule in (10). Normalizing the elements of the noise matrix to variance one, (9) can be written in the form

$$\mathbf{Y} = \frac{r}{\sigma} \mathbf{H} \mathbf{S} + \mathbf{W}, \quad (16)$$

The ML decision rule in (10) can be simplified as

$$\hat{\mathbf{S}}_{ML} = \underset{\mathbf{S} \in \mathbb{S}}{\operatorname{argmin}} \left(\frac{r}{\sigma} \|\mathbf{H}\mathbf{S}\|^2 - 2\mathbf{Y}^T \mathbf{H}\mathbf{S} \right). \quad (17)$$

Let $\mathbf{S}_1$ and $\mathbf{S}_2$ denote two transmit signal matrices. The pairwise error probability (PEP) of giving a decision in favor of $\mathbf{S}_2$ when $\mathbf{S}_1$ was transmitted can be written as [12]:

$$PEP\left(\mathbf{S}_1 \rightarrow \mathbf{S}_2 \mid \mathbf{H}\right) = Q\left(\frac{r}{2\sigma} \|\mathbf{H}\left(\mathbf{S}_2 - \mathbf{S}_1\right)\| \right). \quad (18)$$

An upper bound on the BER can be obtained using union bound as

$$p_e \leq \frac{1}{|\mathbb{S}|MN} \sum_{i=1}^{|\mathbb{S}|} \sum_{j=1,i\neq j}^{|\mathbb{S}|-1} PEP\left(\mathbf{S}_i \to \mathbf{S}_j \mid \mathbf{H}\right) \frac{d\left(\mathbf{S}_i, \mathbf{S}_j\right)}{\eta}$$

$$= \frac{1}{|\mathbb{S}|MN} \sum_{i=1}^{|\mathbb{S}|} \sum_{j=1,i\neq j}^{|\mathbb{S}|-1} Q\left(\frac{r}{2\sigma} \|\mathbf{H}\left(\mathbf{S}_j - \mathbf{S}_i\right)\|\right) \frac{d\left(\mathbf{S}_i, \mathbf{S}_j\right)}{\eta},$$

(19)

where $d\left(\mathbf{S}_i, \mathbf{S}_j\right)$ is the Hamming distance between bit mappings corresponding to the signal matrices $\mathbf{S}_i$ and $\mathbf{S}_j$, and η is the achieved rate of the system.

B. Normalized minimum distance of received signal sets

Here, we obtain a metric based on the ratio of the normalized minimum distances of the received signal sets of different schemes in order to compare their performance. We use this metric to assess the relative high-SNR performance of difference schemes. Suppose $\mathbb{S}_{tx} = \{\mathbf{S}_1, \mathbf{S}_2, \cdots, \mathbf{S}_K\}$ is the set of all possible transmit signal matrices of a particular scheme, where K is the size of the signal set. Let $\mathbb{S}_{rx} = \{\mathbf{H}\mathbf{S}_1, \mathbf{H}\mathbf{S}_2, \cdots, \mathbf{H}\mathbf{S}_K\}$ be the corresponding received signal set in the absence of noise for a given $\mathbf{H}$. The matrices in the set $\mathbb{S}_{rx}$ are normalized by the average received signal power to obtain the normalized received signal set $\tilde{\mathbb{S}}_{rx}$ as $\tilde{\mathbb{S}}_{rx} = \{\tilde{\mathbf{Y}}_1, \tilde{\mathbf{Y}}_2, \cdots, \tilde{\mathbf{Y}}_K\}$, where

$$\tilde{\mathbf{Y}}_i = \frac{\mathbf{H}\mathbf{S}_i}{\sqrt{\frac{1}{KN_rMN} \sum_{i=1}^{K} \|\mathbf{H}\mathbf{S}_i\|^2}}.$$

(20)

The minimum distance of the normalized received signal set $\tilde{\mathbb{S}}_{rx}$ can be obtained as

$$d_{\min,\mathbf{H}} = \min_{\tilde{\mathbf{Y}}_i, \tilde{\mathbf{Y}}_j \in \tilde{\mathbb{S}}_{rx}, i\neq j} \|\tilde{\mathbf{Y}}_i - \tilde{\mathbf{Y}}_j\|_2.$$

(21)

Suppose $\mathbb{S}_{tx_1}$ and $\mathbb{S}_{tx_2}$ are the transmit signal sets of two different schemes. For a given $\mathbf{H}$, let $d_{\min,\mathbf{H}}^{(1)}$ and $d_{\min,\mathbf{H}}^{(2)}$ denote the minimum distances of their corresponding normalized received signal sets. Then, at high SNRs, the BER performance of scheme 1 with signal set $\mathbb{S}_{tx_1}$ will be better than that of scheme 2 with signal set $\mathbb{S}_{tx_2}$, if $d_{\min,\mathbf{H}}^{(1)} > d_{\min,\mathbf{H}}^{(2)}$. The ratio of the minimum distances gives the SNR gap between their BER performance at high SNRs, i.e., the SNR gap in dB is given by

$$\text{SNR}_{\text{gap}} = 20 \log \left(d_{\min,\mathbf{H}}^{(1)} / d_{\min,\mathbf{H}}^{(2)}\right).$$

(22)

Using the above, we can capture the relative performance of different schemes at different spatial positions of the receiver across the room.

V. RESULTS AND DISCUSSIONS

In this section, we present the analytical and simulation results on the BER performance of NDC-OTFS and DCM-OTFS in comparison with those of NDC-OFDM and DCM-OFDM. Performance comparison between NDC-OTFS and DCM-OTFS is also made. The simulation parameters used are summarized in Table I.

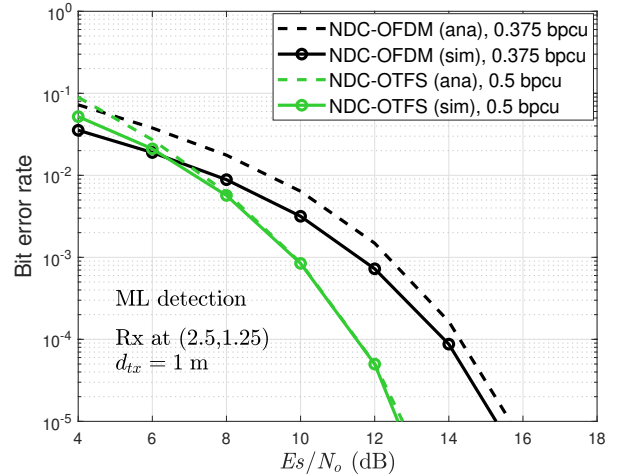|			
Room		Length	5 m
		Width	5 m
		Height	3.5 m
Transmitter		Height from the floor	3 m
		Number of LEDs, N_t	2
		Elevation	$-90°$
		Azimuth	$0°$
		$\Phi_{1/2}$	$60°$
		Mode number, n	1
		d_{tx}	1 m
Receiver		Height from the floor	0.8 m
		Number of PDs, N_r	4
		Elevation	$90°$
		Azimuth	$0°$
		Responsivity, r	0.4 Amps/Watt
		FOV	$85°$
		d_{rx}	0.1 m

TABLE I: System parameters used in the simulations.

Fig. 5: BER performance of NDC-OTFS ($M = 2$, $N = 4$, 4-QAM, 0.5 bpcu) and NDC-OFDM ($M = 8$, BPSK, 0.375 bpcu) with Rx located at (2.5,1.25).

A. NDC-OTFS/DCM-OTFS vs NDC-OFDM/DCM-OFDM

Figure 5 shows the simulated BER performance of NDC-OTFS scheme with $M = 2$ delay bins, $N = 4$ Doppler bins, 4-QAM, and 0.5 bpcu rate. The performance of this scheme is compared with that of NDC-OFDM with $M = 8$ subcarriers, BPSK, and 0.375 bpcu. The d_{tx} value used is 1 m. The (X_R, Y_R) coordinate of the receiver location is (2.5,1.25). The analytical upper bounds on the BER are also plotted for comparison. It can be seen that, as expected, the bounds are tight at high SNRs. It can also be seen that though NDC-OTFS has a higher rate of 0.5 bpcu (compared to 0.375 bpcu of NDC-OFDM), it achieves better performance compared to NDC-OFDM. For example, at a BER of 10^{-5}, NDC-OTFS has an SNR gain of about 2.5 dB compared to NDC-OFDM.

Figure 6 shows the BER performance of DCM-OTFS with $M = 2$, $N = 4$, BPSK, and 1 bpcu. The performance of DCM-OFDM with $M = 8$, BPSK, and 1 bpcu is also shown for comparison. The receiver is located at (2.5,1.25) and the d_{tx} value used is 1 m. It can be seen that DCM-OTFS outperforms DCM-OFDM by about 5 dB at 10^{-5} BER.
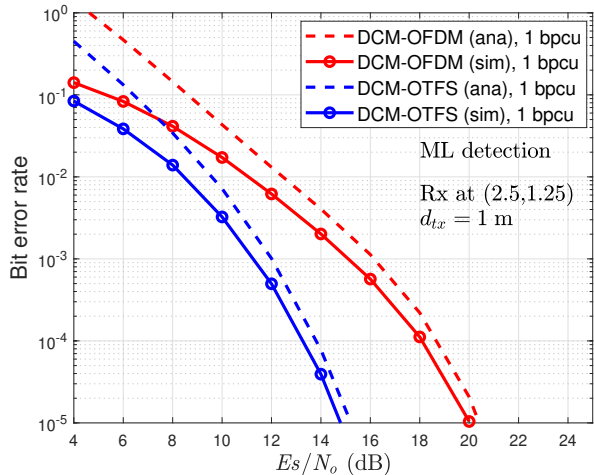
Fig. 6: BER performance of DCM-OTFS ($M = 2$, $M = 4$, BPSK, 1 bpcu) and DCM-OFDM ($M = 8$, BPSK, 1 bpcu) Rx located at (2.5,1.25).
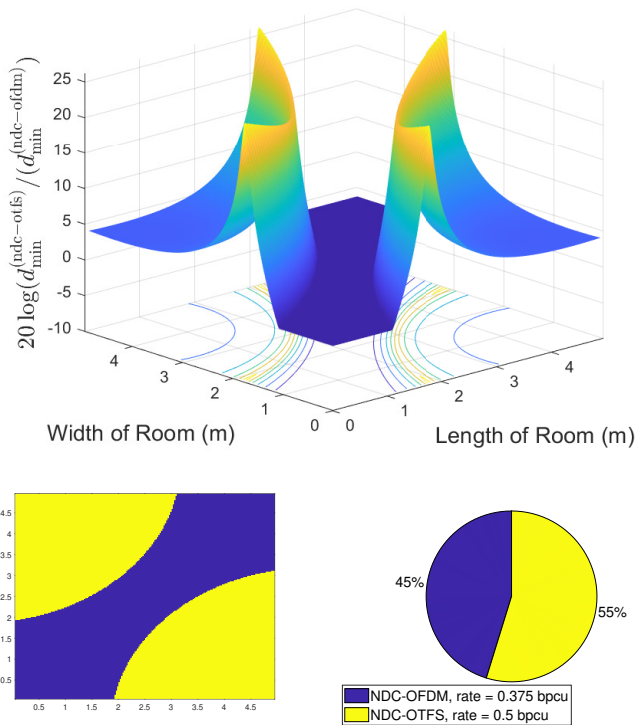

Fig. 7: Spatial distribution of relative normalized $d_{\min}$ of NDC-OTFS with 0.5 bpcu and NDC-OFDM with 0.375 bpcu.

B. Spatial distribution of relative performance

In this subsection, we compare the spatial characterization of the achieved performance of the proposed schemes relative to NDC-OFDM and DCM-OFDM. As mentioned in the previous section, the scheme having a higher normalized $d_{\min}$ value will have better BER performance in the high-SNR regime. We use this to analyze the relative performance of different schemes. Specifically, we plot the SNR gap between
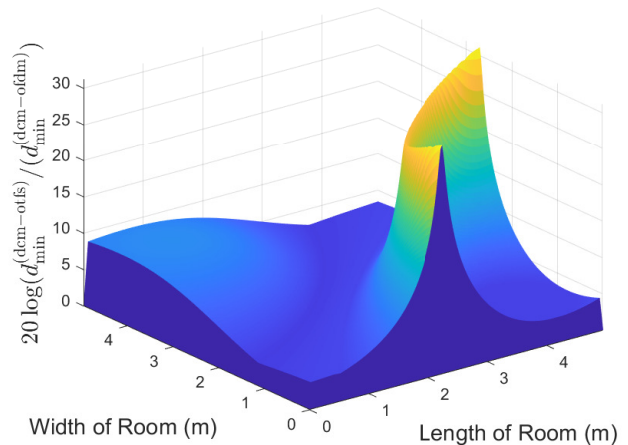

Fig. 8: Spatial distribution of relative normalized $d_{\min}$ of DCM-OTFS with 1 bpcu and DCM-OFDM with 1 bpcu.

two schemes evaluated at different locations of the receiver across the room. For a given receiver location in the receiver plane (0.8 m above the floor), the SNR gap between the two schemes under comparison is computed using (22).

Figure 7 shows the plot of SNR gap (in dB) between NDC-OTFS scheme with 0.5 bpcu and NDC-OFDM scheme with 0.375 bpcu at various locations of the receiver across the room. The system parameters used are as given in Table I. The receiver is placed at a spatial resolution of 2.5 cm across the room. In Fig. 7, we observe that the SNR gap between the considered NDC-OTFS and NDC-OFDM schemes can be of positive or negative dB values across the room. A positive dB value of SNR gap at a receiver location implies that NDC-OTFS performs better than NDC-OFDM in that location. Such locations are marked in yellow color in the receiver plane. Likewise, a negative dB value implies NDC-OFDM performs better, and such locations are marked in blue color. The SNR gain of NDC-OTFS in Fig. 5 at 10^{-5} BER at receiver location (2.5,1.25) corroborates with the SNR gap in favor of NDC-OTFS in Fig. 7 predicted by (22) at this location. It can also be seen that although the rate in NDC-OTFS scheme is high (0.5 bpcu) compared the rate in NDC-OFDM scheme (0.375 bpcu), NDC-OTFS performs better in 55% of the room (see the pie chart). Figure 8 shows a similar spatial performance comparison between DCM-OTFS and DCM-OFDM, both having 1 bpcu rate. We observe that there is positive SNR gap in favor of DCM-OTFS compared to DCM-OFDM in all the receiver locations across the room. Here again, the SNR gap predicted in favor of DCM-OTFS in Fig. 7 at receiver location (2.5,1.25) corroborates with the SNR gain of DCM-OTFS in Fig. 6 at 10^{-5} BER in the same location.

VI. CONCLUSIONS

We investigated the use of the recently introduced OTFS modulation in indoor multi-LED VLC systems. We proposed two dual-LED schemes, namely, NDC-OTFS and DCM-OTFS

schemes, and evaluated their bit error performance through analysis and simulations. While NDC-OTFS used 2D Hermtitian symmetry operation to obtain real-valued signals, DCM-OTFS avoided it through polar representation of complex signals. Also, both the proposed schemes did not need DC bias to generate positive signals compatible for optical transmission. Our simulation results showed superior performance of NDC-OTFS and DCM-OTFS compared to NDC-OFDM and DCM-OFDM, respectively. The spatial distribution of the relative performance of NDC-OTFS/DCM-OTFS and NDC-OFDM/DCM-OFDM was obtained using the ratio of normalized minimum distances of the received signal sets as a metric. These spatial distribution plots revealed the SNR gain/loss of NDC-OTFS/DCM-OTFS compared to NDC-OFDM/DCM-OFDM. The promising performance of OTFS reported in this paper can motivate further research on other MIMO VLC architectures using OTFS.

REFERENCES

[1] P. H. Pathak, X. Feng, P. Hu, and P. Mohapatra, "Visible light communication, networking, and sensing: a survey, potential and challenges," *IEEE Commun. Surveys & Tutorials*, vol. 17, no. 4, pp. 2047-2077, 2015.

[2] A. Memedi and F. Dressler, "Vehicular visible light communications: a survey," *IEEE Commun. Surveys & Tutorials*, vol. 23, no. 1, pp. 161-181, 2021.

[3] Z. Wang, Q. Wang, W. Huang, and Z. Xu, *Visible Light Communications: Modulation and Signal Processing*, Wiley-IEEE Press, 2018.

[4] T. Fath and H. Haas, "Performance comparison of MIMO techniques for optical wireless communications in indoor environments," *IEEE Trans. Commun.*, vol. 61, no. 2, pp. 733-742, Feb. 2013.

[5] S. P. Alaka, T. Lakshmi Narasimhan, and A. Chockalingam, "Generalized spatial modulation in indoor wireless visible light communication", *IEEE GLOBECOM'2015*, Dec. 2015.

[6] O. Gonzlez, R. Prez-Jimnez, S. Rodriguez, J. Rabadn, and A. Ayala, "OFDM over indoor wireless optical channel," *Proc. IEE Optoelectron.*, vol. 152, no. 4, pp. 199-204, Aug. 2005.

[7] J. Armstrong and A. J. Lowery, "Power efficient optical OFDM," *Electron. Lett.*, vol. 42, no. 6, pp. 370-372, Mar. 2006.

[8] N. Fernando, Y. Hong, and E. Viterbo, "Flip-OFDM for optical wireless communications", *IEEE ITW'2011*, pp. 5-9, Oct. 2011.

[9] Y. Li, D. Tsonev, and H. Haas, "Non-DC-biased OFDM with Optical Spatial Modulation," *IEEE PIMRC'2013*, pp. 486-490, Sep. 2013.

[10] S. P. Alaka, T. L. Narasimhan, and A. Chockalingam, "Coded index modulation for non-DC-biased OFDM in multiple LED visible light Communication," *IEEE VTC'2016-Spring*, pp. 1-5, May 2016.

[11] R. Tejaswi, T. L. Narasimhan, and A. Chockalingam, "Quad-LED complex modulation (QCM) for visible light wireless communication," *IEEE WCNC'2016*, pp. 1-6, Apr. 2016.

[12] T. L. Narasimhan, R. Tejaswi, and A. Chockalingam, "Quad-LED and dual-LED complex modulation for visible light communication," available online: arXiv:1510.08805v3 [cs.IT] 24 Jul 2016.

[13] R. Hadani et al., "Orthogonal time frequency space modulation," *IEEE WCNC'2017*, pp. 1-6, Mar. 2017.

[14] R. Hadani et al., "Orthogonal time frequency space modulation," available online: arXiv:1808.00519v1 [cs.IT] 1 August 2018.

[15] K. R. Murali and A. Chockalingam, "On OTFS modulation for high-Doppler fading channels," *ITA'2018*, pp. 1-10, Feb. 2018.

[16] P. Raviteja, K. T. Phan, Y. Hong, and E. Viterbo, "Interference cancellation and iterative detection for orthogonal time frequency space modulation," *IEEE Trans. Wireless Commun.*, vol. 17, no. 10, pp. 6501-6515, Oct. 2018.

[17] P. Raviteja, E. Viterbo, and Y. Hong, "OTFS performance on static multipath channels," *IEEE Wireless Commun. Lett.*, vol. 8, no. 3, pp. 745-748, Jun. 2019.

[18] J. Zhong, J. Zhou, W. Liu, and J. Qin, "Orthogonal time-frequency multiplexing with 2D Hermitian symmetry for optical-wireless communications," *IEEE Photon. Jl.*, vol. 12, no. 2, pp. 1-10, Apr. 2020.

[19] J. Barry, J. Kahn, W. Krause, E. Lee, and D. Messerschmitt, "Simulation of multipath impulse response for indoor wireless optical channels," *IEEE J. Sel. Areas in Commun.*, vol. 11, no. 3, pp. 367-379, Apr. 1993.

[20] J. M. Kahn and J. R. Barry, "Wireless infrared communications," *Proc. IEEE*, vol. 85, no. 2, pp. 265-298, Feb. 1997.